Neuron, Vol. 24, 791–802, December, 1999, Copyright ©1999 by Cell Press

Imaging Cortical Dynamics at High Spatial and Temporal Resolution with Novel Blue Voltage-Sensitive Dyes

Neurotechnique

Doron Shoham, Daniel E. Glaser, Amos Arieli, Tal Kenet, Chaipi Wijnbergen, Yuval Toledo, Rina Hildesheim, and Amiram Grinvald*
Department of Neurobiology
Weizmann Institute of Science
Rehovot 76100
Israel

Summary

Conventional imaging techniques have provided high-resolution imaging either in the spatial domain or in the temporal domain. Optical imaging utilizing voltage-sensitive dyes has long had the unrealized potential to achieve high resolution in both domains simultaneously, providing subcolumnar spatial detail with millisecond precision. Here, we present a series of developments in voltage-sensitive dyes and instrumentation that make functional imaging of cortical dynamics practical, in both anesthetized and awake behaving preparations, greatly facilitating exploration of the cortex. We illustrate this advance by analyzing the millisecond-by-millisecond emergence of orientation maps in cat visual cortex.

Introduction

Sensory perception and higher cortical functions emerge from intricate, dynamic interactions in very large cortical networks. Therefore, understanding of the functioning of a cortical area requires following the dynamics of neuronal population activity with high spatial and temporal resolution. Although this need has long been recognized, existing techniques have forced researchers to focus on either the spatial or the temporal aspects of cortical function.

In the spatial domain, techniques relying on the metabolic consequences of changes in neuronal activity have excellent spatial resolution, but they share a common limitation in the time domain. This family includes 2-deoxyglucose mapping (2-DG), positron emission tomography (PET), optical imaging of intrinsic signals (OIIS), near infrared spectroscopy (NIRS), and functional magnetic resonance imaging (fMRI). The metabolic signals to which these techniques are sensitive are slow relative to the neuronal activity. Thus, none of the existing metabolism-based imaging techniques currently offers temporal resolution better than hundreds of milliseconds.

On the other hand, conventional techniques that do provide temporal resolution in the millisecond range suffer from serious limitations in spatial resolution. Some are essentially point measurements (intracellular recordings, extracellular single or multiunit recordings, or local field potentials). For others, such as electroencephalography (EEG) and magnetoencephalography (MEG), identifying the sources that give rise to the observed signals is fundamentally difficult because the solution to the "inverse problem" is not uniquely defined. Another potentially fast imaging technique could be based on the fast light scattering intrinsic signal, in the millisecond time domain, that has been routinely observed in vitro (Hill and Keynes, 1949; Cohen et al., 1968; Tasaki et al., 1968; Cohen, 1973; Grinvald et al., 1982b). However, this signal has not been exploited for high-resolution in vivo imaging, because it is much smaller than other intrinsic signals. Therefore, it has proven difficult to simultaneously monitor the details of both the "where" and the "when" aspects of neuronal information processing.

Several ongoing research efforts are directed at resolving this conundrum. By combining EEG or MEG with fMRI or PET in humans, some teams are attempting to produce a hybrid technique with high resolution in time and space (George et al., 1995). Although some fundamental issues might limit the actual resolution of these combined approaches, most likely they will prove very fruitful for noninvasive exploration of human higher cognitive functions. Another approach involves large arrays containing dozens of electrodes that record spikes and local field potentials from several square millimeters of cortex (Nicolelis et al., 1997). However, even the largest array provides only a small subsample of the population. Furthermore, field potentials spread far from their site of initiation, effectively limiting spatial resolution.

From the outset, optical imaging based on voltage-sensitive dyes (OIVS) has offered a potential solution to these limitations. The temporal and spatial resolutions of voltage-sensitive dye recordings are limited only by the imaging system and the signal-to-noise ratio (Tasaki et al., 1968; Salzberg et al., 1973; Cohen et al., 1974; Grinvald et al., 1977, 1981, 1983). However, efforts to apply this technique in vivo with natural stimuli have problems with both spatial resolution and the size of activity-dependent dye signals relative to noise (Grinvald et al., 1984; Orbach et al., 1985; Kauer et al., 1987).

Over the past 10 years, we have developed two imaging systems that fit the severe requirements of voltage-sensitive dye imaging discussed below. The first was based on a fast-framing (up to 8 kHz) camera containing a 64 × 64 detector array. With this system, we managed to image orientation maps in cat visual cortex with millisecond time resolution (Shoham et al., 1993, Soc. Neurosci., abstract; Shoham, 1997). Subsequently, a high-resolution fast camera with 128 × 128 detectors was designed by G. Matsumoto, M. Ichikawa, T. Iijima, and their colleagues in the Electrotechnical Laboratory at Tskuba, for imaging in vitro (mainly in brain slices) of voltage and calcium signals (Iijima et al., 1996; marketed as FUJIX HR Deltaron 1700). We modified this system for in vivo dye imaging to produce the data presented in this paper.

In this report, we describe the successful culmination

*To whom correspondence should be addressed (e-mail: amiram.grinvald@weizmann.ac.il).

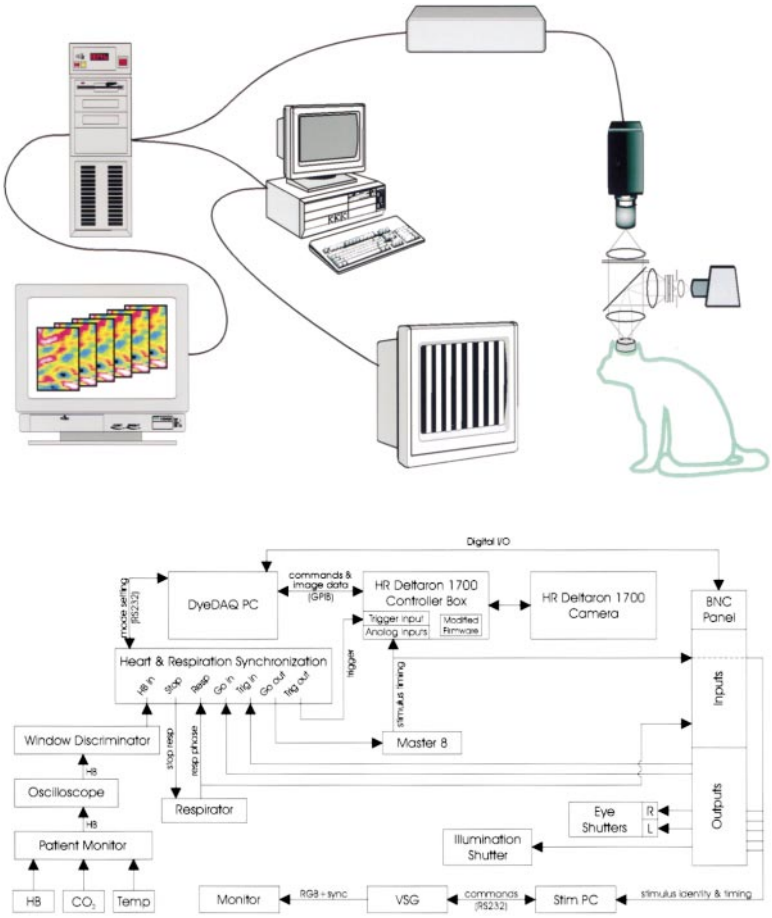

Figure 1. Setup for High-Resolution Dye Imaging

The top panel shows the main system components. The exposed cortex is imaged through a cranial window and a macroscope optical system (Ratzlaff and Grinvald, 1991) by the fast camera. The cortex is illuminated using an epi-illumination stage with appropriate excitation filter and a dichroic mirror. The main computer controls the camera, stores the data, and performs preliminary online data analysis. The visual stimulus is generated by a separate computer and displayed on a monitor. The bottom panel shows a block diagram of the system. The various components are illustrated as boxes, and the interconnections by lines. The DyeDAQ PC at the top of the diagram is the master controller, receiving timing pulses and sending commands to the various subsystems. From left to right, these include a heartbeat monitoring system; a homemade microcontroller box that synchronizes data acquisition to heartbeat and respiration; a respirator that can be halted at a fixed point in the breathing cycle (Ugo Basile 6125); a sequence generator for stimulus timing (Master-8, AMPI); the visual stimulus generator itself, consisting of a control PC, a self-contained stimulus generator box (VSG Series 3, Cambridge Research Systems), and a high refresh rate monitor; controllers for illumination and eye shutters; and finally the camera controller box and the camera itself. Many of these connections run through a BNC panel (far right), which gives the system a degree of modularity. Different stimulating or imaging systems can be substituted for one another in a manner that does not affect other components of the system.

of our efforts to overcome these limitations. By designing novel voltage-sensitive dyes and imaging systems, it has proved possible to directly image activity in cortical columns with millisecond time resolution. With this advanced technology, it is possible to reveal the dynamics of cortical information processing and its underlying functional architecture with the necessary spatial and temporal resolution in both anesthetized and behaving animals. We demonstrate this here with data from cat visual cortex showing the emergence of orientation maps with millisecond time resolution, following the presentation of oriented drifting gratings.

Results

Dye Design Considerations

The previously used dyes were the most important limiting factor responsible for the low signal-to-noise ratio in all previous vertebrate in vivo studies. The low signal-to-noise ratio was problematic because extensive averaging was needed to obtain reliable data. The amount of averaging, and hence illumination time, was limited by photodynamic tissue damage. This made these experiments very difficult in practice. Our solution was to develop better voltage-sensitive dyes.

To understand why the signal-to-noise ratio during in vivo imaging is small, we need to consider the two elements separately, the signals and the noise. The useful voltage-sensitive dye signals come from molecules that are externally bound to the cell membrane, since in this state the dye fluorescence changes linearly with the membrane potential (Cohen et al., 1974; Salzberg et al., 1977). The fluorescence changes resulting from changes in membrane potential are small: the best sensitivity we ever observed was 21%/100 mV for action potentials in clean tissue cultured cells (Grinvald et al., 1983). However, in vivo only a fraction of the dye molecules present in the tissue are actually bound to neuronal membrane: some dye is bound to glia and some remains in the extracellular space, adding a large fluorescence background. Furthermore, at any given moment many of the neurons do not generate action potentials but only synaptic potentials that can be either positive (depolarizing) or negative (hyperpolarizing). These synaptic events constitute a large fraction of the signal, since the dendrites have a relatively large membrane area, at least 50% of the neuronal arborization. Thus, the fractional changes associated with changes in neuronal activity in vivo were small, typically about 1–3 parts in 10,000.

The second element is the noise, which dominates the in vivo imaging experiments. There are many sources of noise ranging from photon shot noise to movement artifacts (Grinvald et al., 1988, 1999). The dominant source of noise in the in vivo experiments was associated with the heartbeat. For example, before processing,

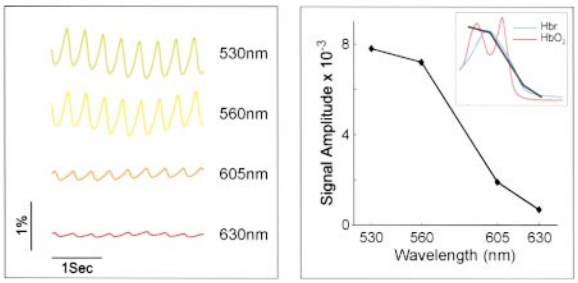

Figure 2. Wavelength Dependency of Heartbeat and Respiration Signals

The left panel illustrates optical reflectance signals from cat visual cortex measured at several wavelengths. The color of the line schematically represents the wavelength of the illuminating light. The signals were averaged over the entire imaged area. The right panel plots the peak-to-peak amplitude as a function of wavelength, illustrating the falloff with increasing wavelength in this range. The inset shows the amplitude plot (normalized) on the same axes as the textbook absorption of oxy- and deoxyhemoglobin, illustrating the close relationship between the two.

the raw data obtained in the past contained a heartbeat signal as high as ten times bigger than the signal evoked by the visual stimulus (Grinvald et al., 1984; Orbach et al., 1985; Shoham et al., 1993, Soc. Neurosci., abstract; Arieli et al., 1995). Although we employ a subtraction procedure to remove the heartbeat signal (which for these experiments is considered as noise), the lack of perfect reproducibility of the heartbeat creates significant artifacts even in the corrected data. Heartbeat signals result from the pumping of blood, and we wondered whether blood volume changes in cortex might be a dominant component. This would be especially serious since the excitation wavelength of the best dye at that time (RH-795) coincides with the peak absorption of hemoglobin. Thus, changes in hemoglobin concentration should strongly affect the number of photons available for dye excitation. If absorption by hemoglobin was indeed the main cause of this disturbing signal, this would suggest an obvious prediction about the dependence of the artifact amplitude on the wavelength of the light used for illumination. However, because there could also be wavelength-independent components, we wanted to assess the actual variation in the size of the heartbeat signal as a function of wavelength.

Wavelength Dependency of the Heartbeat Signal

We used the fast imaging system (Figure 1) to measure cortical reflectance as a function of time. Data acquisition was synchronized to the heartbeat as described above. We changed the wavelength of the illuminating light in an interleaved fashion between short blocks of data acquisition (no stimulus was applied during these recording sessions). From these data, we were able to calculate the amplitude of the changes in reflected light at temporal frequencies coinciding with the heart rate. Figure 2 illustrates a typical example of such an experiment. In the left panel, we present the average change in reflected light over the whole imaged area. The dominant frequency in this signal ($\sim$2.7 Hz) is clearly in the heartbeat range. Each curve presents data from a different illumination wavelength and is schematically color coded. The right panel plots the average modulation depth of the heartbeat signal as a function of wavelength. The two extremes of the curve, at 530 and 630 nm, differ in artifact amplitude by a factor of more than ten. The shorter wavelength was used for excitation of the styryl voltage dyes, such as RH-795, used previously in vivo and an even shorter wavelength for the ANEPPS dye family developed by Loew and colleagues (Fluhler et al., 1985).

For comparison, we also plot the textbook absorption of oxy- and deoxyhemoglobin (inset in Figure 2, right panel). The correspondence between these two curves and that of the artifact amplitude is strikingly good. This shows that indeed the dominant contribution to the heartbeat artifact (during voltage-sensitive dye imaging) is wavelength dependent and blood related. Therefore, we expected that by developing dyes with excitation wavelength outside the peak absorption of hemoglobin, we would significantly improve the signal-to-noise ratio. A series of 79 dyes from the oxonol family (Cohen et al., 1974; Ross et al., 1977; Grinvald and Farber, 1981; Gupta et al., 1981) with excitation wavelengths in the red range (above 620 nm) were synthesized (R. H. and A. G., unpublished data). The screening procedure used to evaluate these dyes is described in the Experimental Procedures section.

Imaging System

Optical imaging of fast voltage-sensitive dye signals poses critical demands on the photosensors. The first issue is spatial resolution. The first system used for in vivo studies was a photodiode array designed in the Cohen laboratory at Yale University, which had only 128 detectors (Grinvald et al., 1981). To examine features of cortical architecture at the spatial scale of the cortical column, one needs a detector array with much higher resolution. The low spatial resolution severely constrained the size of the cortical region whose columnar organization could be studied. For example, Orbach et al. (1985) and Grinvald et al. (1986) imaged a single barrel, studying an area of about 3 $\times$ 3 mm with each pixel viewing a cortical area of 100 $\times$ 100 mm, and Grinvald et al. (1994) visualized about one and a half cycles of the isoorientation domains in a 2 $\times$ 2 mm patch of cortex (200 $\times$ 200 mm pixels). The improved spatial resolution reported here was accomplished by using a fast camera having over a 100-fold more pixels (128 $\times$ 128), allowing the imaging of finer details in even larger cortical areas than before. Here, we imaged a cortical area of 6 $\times$ 6 mm with each pixel monitoring an area of 50 $\times$ 50 mm.

Another critical demand is for detectors with very high well capacity (i.e., the number of photons that can be accumulated in a pixel before it saturates). Voltage-sensitive dye imaging systems need sufficient sensitivity to detect the small fractional changes associated with the fluorescence signals in vivo (as low as 1:10,000). Due to the statistical nature of light, large numbers of photons must be gathered in order to reveal these changes above the photon noise. For example, measuring a signal of 10^{-4} with a signal-to-noise ratio of 10 requires collecting at least 10^{10} photons. This requires pixels with a very large well capacity. In principle, this can also be

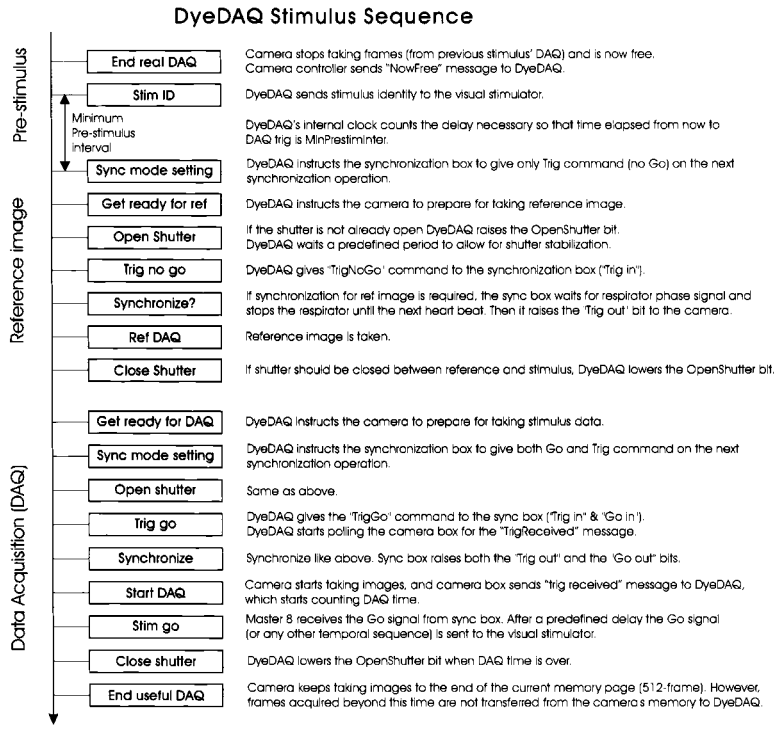

Figure 3. Detailed Timing Sequence for the Stimulus Loop

This is the central control structure that determines the timing of the inner loop in the data acquisition cycle. The complexity of the structure derives from two sources: first, from the need to integrate the functionality of many different systems into a coherent protocol, and second, from the competing range of biological, chemical and physical constraints inherent in voltage–dye imaging. In addition, there is a need to take a reference image with this camera in order to obtain an amplified ($\times 4$ to $\times 64$) differential image prior to the 8-bit digitization. This arrangement provides an effective 12–16 bits accuracy using an 8-bit digitizer. These constraints have been integrated into the architecture and sequencing of the system. See the text for a detailed description.

achieved by binning pixels in space. However, since only limited binning can be done on-chip, this approach requires transferring highly oversampled digital images for off-chip binning. Since voltage–dye imaging needs high frame rates, this would imply extremely fast digitizers and high data transfer rates. It should be noted that the voltage-sensitive dye signal is much smaller than that provided by calcium probes, often by more than 100-fold. Therefore, voltage-sensitive dye imaging makes much more severe demands on the imaging detector (and the unfortunate experimenter). The development of suitable detectors for fast imaging of small signals has been very slow. This is not because of fundamental technical limitations in photosensor technology, but because of the absence of a large market for them.

Technical Description of the In Vivo Imaging System

The fast imaging system was based on the FUJIX HR Deltaron 1700 camera with a hardware and software environment that we developed (Figure 1). The camera offers a variable frame rate of up to 1700 Hz. The main advantage of this camera is the high well capacity of the detector chip (around 10 million electrons/pixel; standard CCD chips have 200,000–700,000), which means that enough photons can be gathered so as to eliminate shot noise as a limiting factor in the experiments. Thus far, the detector in the Fuji camera is the only commercially available detector with such a high dynamic range at the spatial and temporal resolution offered (Iijima et al., 1996).

A schematic view of the entire imaging system is provided at the bottom of Figure 1. The heart of the system is a PC that runs a hybrid Visual C++/Visual Basic software (DyeDAQ). In addition to data acquisition, this PC monitors the other elements of the system, including the camera, a patient monitor, a respirator, a synchronization circuit (see below), the stimulus generator, and the illumination controller. The PC also sends control and timing pulses. Figure 3 illustrates the central control structure of the DyeDAQ software.

To reduce the fast large noise from heart pulsation, the data acquisition was synchronized with heartbeat detected from the electrocardiogram (ECG), and a subtraction procedure was subsequently used to minimize this noise (Grinvald et al., 1984). Furthermore, to minimize the slow noise from the animal respiration, we synchronized the respiration cycle to the heartbeat as well, in each cycle of the data acquisition. The respirator was stopped immediately before the onset of data acquisition and released on the next heartbeat detection, thus synchronizing data acquisition to both the respiration and the heart cycles. Therefore, the same subtraction procedure effectively minimized also this large and slow respiratory noise (Grinvald et al., 1994). This synchronization procedure is the most timing-critical phase of the experiment, since the success of the subtraction procedure depends on the synchronization accuracy. To ensure a reliable process, we implemented it using a dedicated microcontroller-based circuit, which produced the actual timing pulses.

The biggest single limitation of the commercial system is that images cannot be transferred from the camera to the host PC in real time. This is because the transfer is via an old GPIB connection allowing transfer of only 8 images/s, whereas the camera collects up to 1700 images/s. Therefore, images are first stored in the camera's controller memory (3072 frames). In many experiments, it is necessary to use signal averaging. The commercial system allows one to average over several repetitions of each stimulus, before transferring the data

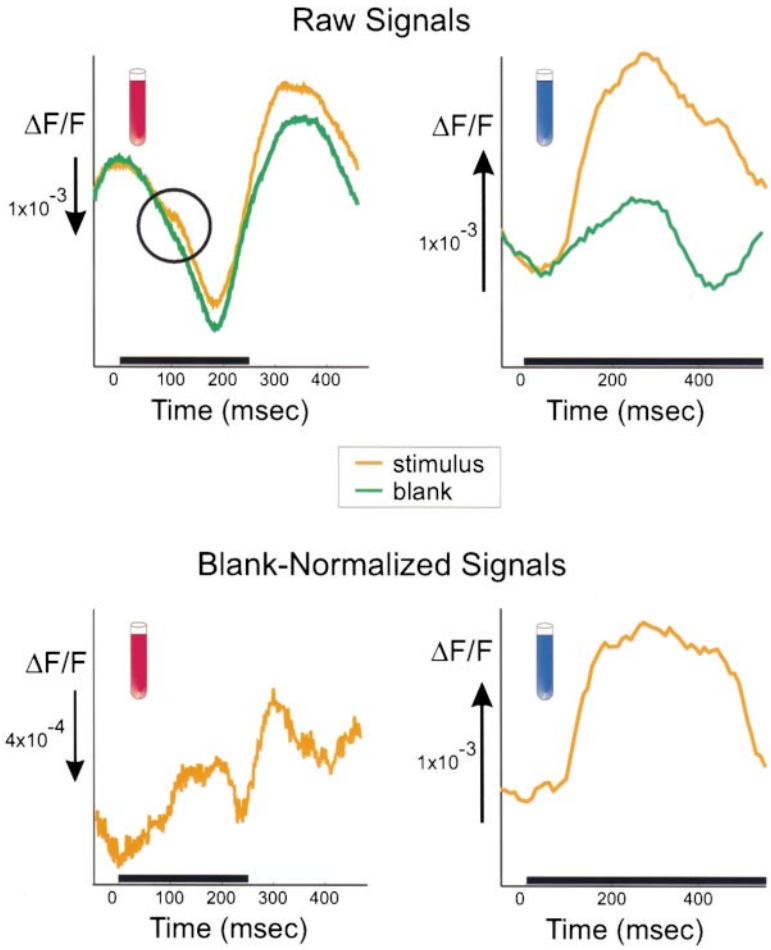

Figure 4. Time Course of the Evoked Voltage-Sensitive Dye Signals

The top panels illustrate the signals from different experiments using the red dye RH-795 and the blue dye RH-1692, respectively. The curves show the raw fluorescence signals, without subtracting the blank, integrated over the imaged area (cat area 18). The orange curves are from the stimulated condition, and the green lines are the blank data (no stimulus). Data acquisition was synchronized to the heartbeat. The solid black line marks the stimulus period. The circle in the left top panel (RH-795) points to the time of the evoked fast signal, showing how small the fast evoked response is relative to the heartbeat signal. Note how much bigger the blue dye–evoked signal is relative to the heartbeat signal (top right). Note also that the absolute magnitude of the evoked signals is larger, yet the major improvement is the relative size of the heartbeat signal and the evoked signal. Note also that the signs of the signals from the two dyes are opposite. The bottom panels show the same data as at the top but with the heartbeat signal (blank) subtracted. Note the large heartbeat artifact with the red dye at the time of the second heartbeat. Again, the blue dye produces a much better signal-to-noise ratio, allowing examinations of small components in the response and longer recording interval that are still reliable. In both cases, 16 presentations were averaged.

slowly to disk. However, stimulus order cannot be randomized. Randomization of stimulus order is essential to eliminate systematic errors originating from the preceding stimulus conditions, whether due to intrinsic signals or to slow components of the neuronal activity. To overcome this limitation, we redesigned the logic of the camera's control system. The firmware that controls the microcontroller in the camera was modified and programmed into a new EPROM chip. This modification resulted in a large reduction in the duration of the experiment, since the data acquisition–to–data transfer ratio was increased (e.g., 64-fold when averaging 64 trials/experiment).

Experimental Results

The dye screening (see Experimental Procedures below) resulted in a few candidate dyes, and we chose to proceed with the novel oxonol dye named RH-1692 (R. H. and A. G., unpublished data). We illuminated the cortex using a 630 $\pm$ 10 nm filter, and collected light at wavelengths above 665 nm. We imaged the responses in cat areas 17 and 18 to visual stimuli consisting of high-contrast moving gratings. We first considered the evoked response calculated as the mean fluorescence change over the entire imaged area. Figure 4 illustrates the type of signals we obtain in cat experiments. The top panels show the novel blue dye responses as a function of time (right), compared with the previous red voltage-sensitive dye RH-795 (left). To show the corresponding amplitude of the heartbeat signal, we also plot the signal obtained in a "blank" condition, which was also synchronized to the heartbeat but with no stimulus (green traces). The improvement in the quality of the evoked signal resulting from the new excitation wavelength is evident. The evoked response is clearly visible even without subtracting the blank. As predicted by the wavelength measurements described above, the heartbeat artifact in the signal from RH-1692 was over 3-fold smaller than the evoked signal. By contrast with the RH-795 data, the artifact was about 5-fold higher than the signal. Also illustrated is the blank-subtracted data, which does succeed in eliminating some residual heartbeat signal (Figure 4, bottom panels). Overall, it appears that this novel dye provides a very large improvement of signal-to-noise ratio compared to the old dyes. In addition to the 5- to 10-fold decrease of the heartbeat noise, there was also a 2- to 3-fold increase of the signal size due to an increased voltage sensitivity of the dye. Thus, the novel dye provides a 10- to 30-fold improvement in the signal-to-noise ratio.

Next, we examined the spatial extent of the response. For each time after stimulus onset, we calculated the ratio of the image obtained following the onset of an oriented grating to that obtained in a blank case (Figure 5). This normalized for nonuniformity of the illumination and staining density. Since data acquisition in all cases

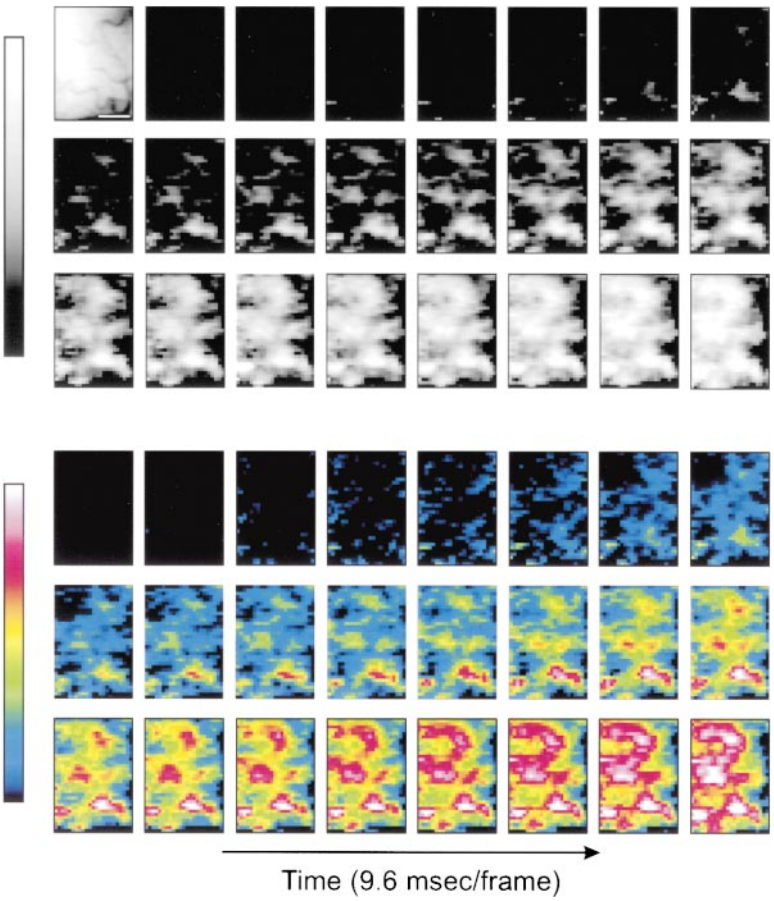

Figure 5. Spatiotemporal Pattern of the Evoked Signals

Images of stimulus-evoked cortical activity in cat area 18. The first frame in the sequence shows an image of the cortical surface (left hemisphere) obtained with green light (540 nm) to emphasize the blood vessel pattern. The scale bars here and in the following figures are 1 mm. The remaining sequence of frames shows the fast fluorescence signals (from RH-1692), which were evoked by stimulation with a left-oblique grating. Each frame is the result of dividing the image obtained in response to the onset of the stimulus by the corresponding image obtained with no stimulus (blank). To remove residual slow noise, the average of the images from 200 ms before stimulus onset was subtracted from each of the subsequent frames. Data were collected at a rate of 833 frames/s and were binned offline in time to 9.6 ms/frame for presentation here. The stimulus onset (time 0) was at the beginning of the first frame. The maps are the average of 16 presentations. The same data is reproduced in the lower time sequence but with a color scale. In both cases, the full range of the color scale corresponds to a fractional change of 0.9×10^{-3}. Note the patchy appearance of the activity in these single-condition maps, which begins at around 80 ms and shows up as brightening in the image. This latency varied between animals in the range of 55–90 ms.

was synchronized with the heartbeat, this procedure also removed any reproducible spatiotemporal pattern associated with the heartbeat. Since this dye responds to membrane depolarization by an increase in fluorescence, the activation of the cortex is visualized as brightening in the images. The activation of the cortex is evident over the whole imaged area from about 80 ms after stimulus onset, and it peaks about 120 ms later.

The activation in these so-called "single-condition" maps is clearly not spatially uniform. To check the nature of the patches in such single-condition maps, we summed up the frames between 100 and 180 ms after stimulus onset (from another cat; Figure 6, left panel). We separately processed the responses to the orthogonal orientation (Figure 6, middle panel). These were compared with a differential orientation map obtained from the same cortex before dye application using standard methods of intrinsic imaging (Figure 6, right panel). The correspondence between the light (activated) patches in the voltage–dye maps and the corresponding orientation domains in the intrinsic maps is illustrated by colored crosses. Incidentally, only in the very best intrinsic signal experiments can clear single-condition orientation maps be obtained. Such dye maps had been obtained previously using RH-795 and our 64 × 64 fast camera (MR6464, Adaptive Optics/EG&G), but their quality was substantially lower (Shoham et al., 1993, Soc. Neurosci., abstract; Shoham, 1997).

To emphasize the difference between two maps produced from orthogonal stimulus orientations and to visualize more clearly the orientation-specific component of the response, we calculated the time series of differential orientation maps from the voltage–dye signals (Figure 7). Clear functional domains are visible in this "movie." These maps can, in the best cases, be detected from a single presentation of each orientation. They clearly resemble the intrinsic signal maps (Figure 8). It should be noted that, as stated above, depolarization causes fluorescence increase and hence lightening with RH-1692, but that intrinsic signals manifest an absorption increase and hence darkening with increased activity. Thus, the intrinsic maps presented in this (and indeed the previous) figure are "reversed": where the dye maps present left over right oblique conditions, the intrinsic maps are right over left obliques. In both cases, the order is arbitrary, and this convention makes the similarities between the functional domains obtained with the two techniques clear.

Since an absorption change at either the excitation or the emission wavelengths will affect the number of photons reaching the detector, intrinsic signals can contaminate what is supposed to be a fluorescence measurement of membrane potential changes. Despite the existence of fast intrinsic signals in vitro (Grinvald et al., 1982b), they are too small to be detected in vivo and thus do not contaminate the fast dye response. However, the slow intrinsic signals have a much higher amplitude, and they are commonly used for functional imaging in vivo (Grinvald et al., 1986; Frostig et al., 1990; for a recent review, see Grinvald et al., 1999). These slow signals can easily be seen in fluorescence measurements when the response is recorded for a longer

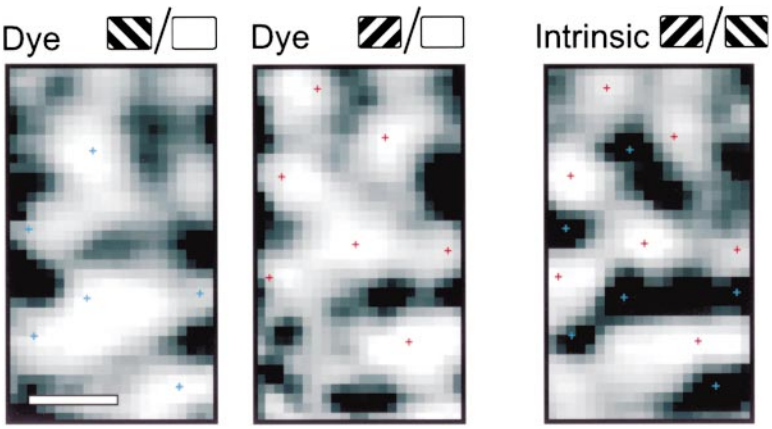

Figure 6. Comparing the Voltage Dyes Single Condition-Maps to the Differential Orientation Map from Intrinsic Signals

The leftmost panel depicts the voltage–dye single-condition map obtained by summing the frames from times 100 ms to 180 ms. The data is taken from a similar experiment to that shown in Figure 5, performed on another cat in which intrinsic imaging was also carried out. The center panel depicts a similar map obtained with the orthogonal stimulus. Note the complementary nature of these two single-condition maps. The rightmost panel depicts a differential orientation map obtained using intrinsic signals before the cortex was stained. The image obtained with a right oblique grating is divided by the image from a left oblique grating, and the resulting map of orientation preference is coded in the gray scale. The blue and red crosses (which are in the same position in all the images) aid comparison of the maps. It is clear that the white patches representing depolarization in the dye single-condition map (middle panel) correspond to the appropriate patches in the intrinsic signals differential orientation map.

period. Figure 9 presents a recording of fluorescence using voltage-sensitive dye RH-1692, where the duration of the recording was extended to several seconds. After the initial fast evoked response due to the voltage signal, there is a large negative signal peaking around 3 s after stimulus onset, corresponding to the known sign and time course of intrinsic signals. Measurements of intrinsic signals in other experiments have shown that their onset latency is ~200–300 ms, and therefore the contamination of the voltage-sensitive dye signals begins at this time. We verified in this and other experiments that the first fast component does not appear in a reflectance measurement without dye.

Other Effects of the Dye

As mentioned above, the limiting factor with many previous dyes was the phototoxicity often referred to as photodynamic damage (Ross et al., 1977; Grinvald et al., 1988). We had evidence from the screening procedures that the novel oxonol dye RH-1692 is no more phototoxic than previous styryl dyes like RH-795. The improved signal-to-noise ratio means that high-quality images can be obtained with fewer trials and hence less illumination than with previous dyes. Nevertheless, we checked the functioning of the cortex during and after the voltage–dye imaging. The tests described below also control for pharmacological side effects.

Firstly, we measured intrinsic signals after the end of the voltage–dye imaging session. High-quality orientation maps were obtained, indicating that cortical circuitry supporting orientation selectivity was functioning normally. This is an important indicator of the overall well-being of the cortical tissue. The existence and quality of the intrinsic signal maps depend also on the proper functioning of metabolic and microcirculatory regulation mechanisms. Thus, this test indicated that the cortex was in good physiological condition throughout the voltage–dye imaging. We also used standard extracellular recording of spikes of single and multiunits and local field potential (LFP) and EEG during and after the imaging session. Here again, we found no evidence of deterioration, and good selectivity for orientation was reliably obtained.

In addition to the above tests in several experiments, we recorded intracellularly membrane potential simultaneously with the voltage–dye imaging as part of an another project with I. Lampl and D. Ferster from Northwestern University (A. Sterkin, I. Lampl, D. Ferster, D. E. G., A. G., and A. A., unpublished data; Sterkin et al., 1999). While monitoring synaptic potentials and action potentials, we found no deterioration or abnormal response properties throughout the experiments.

We found, however, that the amplitude of the evoked voltage–dye signals did decrease over time. Part of this

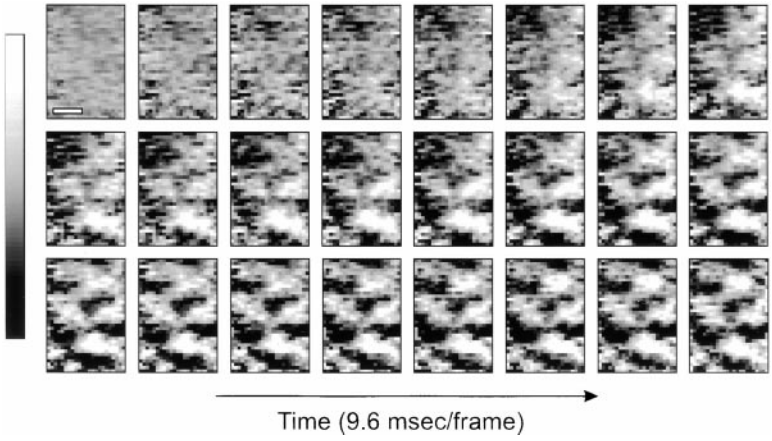

Figure 7. Imaging Orientation Maps with Millisecond Time Resolution

A sequence of differential images obtained by dividing each image from Figure 5 by the corresponding image from the orthogonal stimulus. Light patches in a given map correspond to regions that responded better to left oblique gratings at that time, and dark patches to right oblique. The full range of the gray scale corresponds to a fractional change of 1.2×10^{-3}. With RH-1692, we observed orientation maps with amplitude of up to 1.5×10^{-3}.

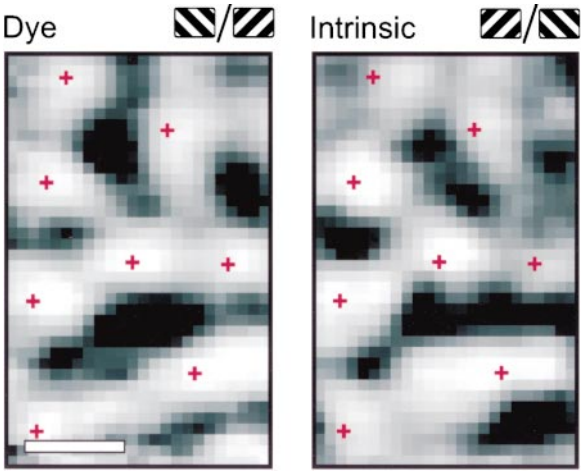

Figure 8. Comparison of Intrinsic and Dye Maps from the Same Cortex

The differential intrinsic map (Figure 6) is compared to the dye differential map obtained from the two single-condition measurements (Figure 6). Note that the "sign" of the maps is reversed by reversing the conditions in the numerator and denominator, since in intrinsic signals darkening represents activity increase, whereas in the blue dye signals depolarization causes whitening.

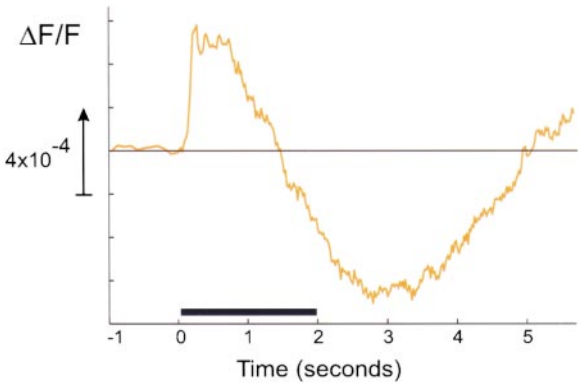

Figure 9. The Dye Fluorescence Also Reflects the Slow and Delayed Intrinsic Signals

The curve shows blank-subtracted fluorescence signals integrated over the entire imaged area in an experiment with long stimulus and data acquisition. The solid black line marks the stimulus period (2 s). Two components are evident in the response: first, the fast positive signal from the voltage-sensitive dye, and later (~750 ms after stimulus onset), the appearance of a negative signal. The latter component is due to increased absorption of the tissue at the excitation wavelength of the dye, and hence indirectly reflects the intrinsic signals. This component is independent of the dye voltage-dependent signals. Note that the time-to-peak of the delayed component, around 3 s, is typical of the well-known intrinsic signals as measured without dyes.

decrease was associated with a decrease in the overall level of the fluorescence as a result of dye bleaching or unbinding. In a typical experiment, 30 min to 1 hr of continuous illumination would bleach the dye completely. Note that this is the total illumination time, not elapsed time. This duration is long enough for signal averaging of several thousand trials. We also found that the dye signals from a stained cortex deteriorated 6–10 hr after the end of the cortical staining, even without any illumination. In some of these cases, we restained the cortex for a second time, and large signals were observed again, indicating the photodynamic damage or pharmacological side effects were not the limiting factors of these experiments.

Discussion

The Novel Dye

A significant advance presented in this paper is the novel dye, which is in some senses a chemical engineering solution to a biological problem. In the first in vivo experiments, the voltage–dye signals were clearly visible but the heartbeat pulsation contained fast components that interfered with the fast dye measurements. The subtraction procedure (Grinvald et al., 1984) indeed reduces this artifact considerably but does not eliminate it, particularly if the duration of the trial is much longer than the heartbeat interval. This is because the optical heartbeat signal is not perfectly reproducible from one trial to the next, and because of the common slight variations in the heartbeat frequency. Thus, while the first part of the response is properly corrected, after a few heartbeat cycles the heartbeat is no longer truly synchronized, so the correction is less effective. As we have shown here, the action spectrum of this heartbeat signal appears similar to the absorption spectrum of hemoglobin. The "blue" oxonol dye RH-1692 is a voltage-sensitive dye with an absorption spectrum remote from the peak of hemoglobin absorption that can be reliably employed in vivo. Here, we have presented data to show that this dye offers a 10- to 30-fold improvement in signal-to-noise ratio when compared with previous dyes. With such an improvement, 100–900 times less averaging is needed to obtain an equivalent signal-to-noise ratio. In addition to the cat data shown here, this dye has been successfully employed in anesthetized rat and monkey (unpublished data) and awake behaving monkey (H. Slovin, A. A., and A. G., unpublished data; see also Slovin et al., 1999, 5th IBRO World Congr. Neurosci., abstract). Furthermore, the improvement in signal-to-noise ratio is so large that ongoing cortical population activity could be monitored with an excellent signal-to-noise ratio without signal averaging (A. Sterkin, I. Lampl, D. Ferster, D. E. G., A. G., and A. A., unpublished data; see also Sterkin et al., 1999, 5th IBRO World Congr. Neurosci., abstract). In this last set of experiments, simultaneous imaging of synchronous fluctuations in membrane potential and the intracellular recording from a single cell provided clear-cut evidence that this dye indeed measures changes in membrane potential in vivo.

We found that the pharmacological side effects of this dye are negligible, as demonstrated by the intrinsic imaging that was performed after the end of several dye imaging sessions, and by simultaneous extra- and intracellular recordings that exhibited normal tuning properties of the cells during both spontaneous and evoked activities. Because of the signal-to-noise improvement, much less illumination time was required to obtain reliable maps and single-trial imaging was possible.

It has been explained that even a fluorescence measurement may contain components from intrinsic signals. This potential artifact has been often ignored. The fluorescence change associated with depolarization in the presence of voltage–dye RH-1692 produces an increase in light. This is the opposite of the previous voltage–dye RH-795. Intrinsic signals in vivo have the same sign as RH-795 signal and therefore could not necessarily be distinguished at first sight. Using the novel dye, we can distinguish directly between a dye signal and a fast intrinsic signal purely on the basis of the signal's sign.

Imaging Small Signals at High Spatial and Temporal Resolution

While the imaging system we developed for these experiments is based on an earlier in vitro system developed by G. Matsumoto, M. Ichikawa, T. Iijima, and their colleagues in the Electrotechnical Laboratory at Tskuba, a few details are worth discussing since there is at present no commercially available system that is suitable for this type of in vivo imaging. The heart of the system is the actual detector chip, which employs a "limited-edition" XY-addressable CMOS technology. This offers a well capacity and readout rate that is currently unmatched. Unfortunately, the commercial Fuji System for in vitro imaging suffers from serious limitations. Thus, its use in vivo required considerable modifications of both the hardware and the software. In particular, we found that the data acquisition and data transfer protocols needed to be completely rewritten. These difficulties were overcome, and the system can be readily employed mainly in experiments in which signal averaging is used.

A fundamental limitation of the current system is that the data transfer from the camera's controller memory to the computer is only 8 frames/s. This makes the system very far from optimal for experiments that require trial-by-trial analysis, such as those described in Arieli et al. (1995, 1996). Another very serious limitation of the present system is its large dark noise. Typically, when the light level is 50% of the saturation level, the dark noise becomes the dominant noise. In this regime, when the dark noise dominates, the signal-to-noise ratio scales down linearly with decreasing illumination rather than as the square root. For example, if the light level is 1/10 of the dark noise, the signal to noise will drop by 10 instead of 3.3. This means that to get the same signal-to-noise ratio 10-fold more signal averaging is required, often an impractical solution. Thus, widespread use of this technique in vivo is probably dependent on the next generation of fast cameras, which are currently being developed and are estimated to become commercially available in 1–3 years.

Orientation Maps with Millisecond Time Resolution

The potential of voltage dyes for high spatial and temporal resolution imaging in vivo has been clear for many years. The improvements in dyes and imaging systems described in this paper allowed us to bring this potential to reality and to obtain the high-quality millisecond domain functional maps illustrated in this paper. It should be noted that functional maps with high spatial resolution were studied in the past essentially as static systems. This is because the imaging was based on slow intrinsic signals. Even in some previous studies that utilized voltage-sensitive dyes, the signals obtained were most likely only the intrinsic signals because the time course did not show the early fast component seen in Figure 9 but only the slow component (Blasdel and Salama, 1986). Therefore, the time course of these signals did not reflect the time course of neural activity. By contrast, the technique described here can be used to measure the spatiotemporal structure of the cortical representation of a feature such as orientation. For example, it has been shown that central processing is responsible for a delay of shape perception by a sudden luminance change (Glaser et al., 1998, Neurosci. Lett., abstract).

Using the methodology described in this paper, high spatial and temporal resolution functional maps can be obtained in vivo in a reliable and reproducible manner. The spatial quality of the maps obtained with the novel dye was at least as good as that obtained using intrinsic signals in the same cortex. In the best cases, we were able to obtain maps from single presentations of each of the stimuli. Even in an average experiment, a sufficient map quality can be obtained from a dozen trials, which means that many more stimulus conditions can be presented and explored in the same experiment. Also, the ability to see neuronal activity without averaging significantly contributes to the study of cortical dynamics. Equally important is the ability to explore the dynamics of single-condition maps (e.g., Figure 5) rather than differential maps.

Current Limitations and Future Directions

Improvement of the dye sensitivity is always desirable, and therefore additional efforts in the chemical engineering of even better dyes will be very rewarding. These dyes may be from existing families such as cyanine, merocyanine, oxonol, and styryl dyes (Cohen et al., 1974; Grinvald et al., 1977, 1982a; Ross et al., 1977; Loew et al., 1978; Gupta et al., 1981) or from new families of dyes. A new approach exploiting fluorescence resonance energy transfer between donor and acceptor dyes (FRET) has been introduced recently (Gonzalez and Tsien, 1997). Subsequent application of this dye to the imaging of neural systems (Cacciatore et al., 1999) suggests that the further adaptation of this technique for use in mammalian cortex may be fruitful. An increase in time resolution and the selection of a donor with peak absorption above 630 nm, remote from the hemoglobin excitation, would make this approach suitable for exploring vertebrate brains in vivo. It is also expected that eventually genetic engineering of suitable in vivo probes, which already proved feasible in simple preparations (Miyawaki et al., 1997; Siegel and Isacoff, 1997), may make the experiments much easier and substantially improve the quality of results obtained by this method. It is to be hoped that better dyes for cat and monkey research will be developed using this approach. One obvious advantage of the genetic engineering approach is that it may provide us with probes that are cell type specific.

Similarly, the photosensors and the related hardware can be improved. Efforts along this line have already begun, and it appears that a turnkey fast imaging system will become commercially available in the near future. It should be noted that commercial video-based systems for fast imaging at video rates offer a time resolution of 16.66 or 20 ms. Although this time resolution is not always satisfactory, the pioneering work of Kauer on the salamander olfactory bulb clearly demonstrated the usefulness of dye imaging at video rates in some preparations (Kauer, 1988).

The results reported and discussed here indicate that real time optical imaging has matured to allow explorations of the cortex in ways never feasible before. No alternative imaging technique for visualizing functional organization in the living brain provides a comparable spatial and temporal resolution. It is this level of resolution that allows voltage-sensitive dye imaging to address questions of both where and when processing is performed. To increase the dimensionality of neurophysiological data obtained from the same patch of cortex, real-time optical imaging can be combined with targeted tracer injections, microstimulation, or intracellular and extracellular recordings. These combined approaches address also the fundamental, mechanistic question of how, thus promising that this technique will play a prominent role in the study of neural coding at the population level.

Experimental Procedures

Surgical and Imaging Procedures

We used an acute cat preparation for these experiments. The methods for preparing and maintaining the animals were similar to those described previously (Ts'o et al., 1990; Bonhoeffer and Grinvald, 1993; Bonhoeffer and Grinvald, 1996). Animals were initially anesthetized with ketamine/xylazine intramuscularly and then with intravenous pentothal. The trachea was cannulated and the animal was artificially respirated so as to keep the end tidal CO_2 at 4.5%. The ECG and global EEG were monitored throughout the experiment. A piece of bone was removed, a stainless steel ring was cemented to the skull over the area of interest, and the dura was ressected. The chamber was filled with CSF–PBS. After surgery, animals were paralyzed with succinylcholine hydrochloride. Zero power contact lenses were fitted to the eyes, and separate eyeglasses brought the plane of focus onto a tangent screen. Initially, imaging of intrinsic signals produced baseline orientation maps. Then, the cortex was stained with the voltage-sensitive dye for 2 hr and washed with CSF–PBS. Recordings were performed with either CSF–PBS or silicon oil in the recording chamber. The cortex was illuminated using an epi-illumination system with appropriate pre- and postfilters and a dichroic mirror selected for the particular dye.

Visual Stimuli

The stimuli used were drifting, high-contrast square-wave gratings of optimal spatial and temporal frequencies for the imaged area (typically 0.6 cycles/° and 2 Hz for area 17 and 0.2 cycles/° and 6 Hz for area 18). The stimulus set contained gratings of various orientations, including at least one pair of orthogonal orientations, and a "blank" condition in which the screen was uniformly gray. The screen was also gray (and globally isoluminant with the gratings) during the interstimulus intervals (5–10 s).

The stimuli were displayed using the "STIM" program written by Kaare Christian on a SGT Plus video graphics board (Number Nine Corporation, Cambridge, MA) offering a frame rate of 60 Hz, or using the VSG Series 3 system (Cambridge Research Systems, Cambridge, England). A Sony GDM-20SE2T5 monitor offered a maximum frame rate of 150 Hz at a resolution of 640 × 480 pixels. The refresh rate of the latter system offered two advantages. Firstly, the lower frame rate of the first system can be reflected in neuronal activity. Secondly, since recordings are triggered on the heartbeat, the screen refresh introduces a jitter into the stimulus onset. The screen was generally placed 57 cm from the eye of the animal. The pulses used to initiate stimulus movement and a photodiode pointed at the stimulating screen were used to check the synchronization of the stimulus.

Dye Screening

The dyes were screened in a variety of preparations to assess their suitability for in vivo imaging, i.e., that they were voltage sensitive in vivo and nontoxic, with acceptable photodynamic damage and bleaching, and that they could penetrate and stain deep cortical layers. We employed a series of assays ranging from in vitro screening through the use of vesicles, the isolated optic nerve of neonatal rats, and on to an in vivo rat cortex model using somatosensory or visual stimulation. In addition, candidate dyes were tested at the end of intrinsic signal imaging experiments on both cat and monkey to assess their ability to stain the cortex properly. The in vivo preparation is described here.

Several hundred rats were used for screening the 79 novel dyes. The rats were anesthetized with urethane and a craniotomy was performed over the barrel cortex area. A well around the hole was constructed out of dental cement. The dura was ressected, and a ball electrode was used to record the response evoked by an air puff delivered to the contralateral whiskers. This allowed us to ensure that the stimulus and the preparation were optimized before dye application. The cortex was then stained for 2 hr with a solution of the dye in CSF–PBS diluted to an optical density of between 3 and 6 at 580 nm. To make sure that the dye had not damaged the cortex significantly, after the dye was washed from the cortex the electrical evoked response was checked once more. Then, a microscope was used to focus an image of a 2 mm square region of cortex containing the largest electrical evoked response onto a single photodiode. The cortex was illuminated using a tungsten–halogen lamp, a dichroic mirror, and pre- and post-filters appropriate for the dye. A dedicated hardware controller triggered a set of trials that alternately contained an air puff stimulus or were blank. All trials were synchronized to the heartbeat, and a digital oscilloscope was used to subtract odd and even trials. In this way, the optical evoked response to whisker stimulation could be separated from the heartbeat artifact.

Having established that a given dye produced a nice evoked optical response in rat, we checked whether it also stained the cat and monkey cortices, since in many previous cases there were species-specific differences. We used animals that had undergone intrinsic imaging experiments and stained with the dye as in the previous paragraph. We tested dye staining in 40 cats and 12 monkeys (two to six dyes in each animal). Staining was evaluated by eye using a pair of filters appropriate to the dye, or using the intrinsic imaging system along with an epi-illumination system containing a dichroic mirror. In most cases, after the animal had been given a lethal injection of anesthetic, a piece of cortex was removed and a tangential section cut. This was inspected by eye using standardized fluorescent illumination to reveal the extent of the staining in depth. We found that many dyes did stain the cortex to a depth of at least 1–2 mm.

The best candidate dyes found by the above procedure were finally used to record voltage signals from cat and monkey cortex. We used 30 cats and 4 monkeys for this stage. We checked whether dye signals could be obtained, and more specifically we looked for dye-dependent functional maps. To check for dye pharmacological side effects, we performed intrinsic imaging to obtain the orientation maps before and after using the dye and verified that they did not change as a result of the dye.

Acknowledgments

We thank the Bio-Imaging Systems Division of the FUJI Photo Film Company for their generous assistance in modifying the HR Deltaron 1700 system. We thank Gene Ratzlaff for his crucial contribution to the development of the first high-resolution system, Ziv Gottesfeld

for help in the early development and experiments, Dahlia Sharon for her help in preparing Figures 1 and 3, Alexander Sterkin for help in preparing Figure 4, and Dov Ettner and Edna Segal for excellent technical support. This work was supported by grants from the Joint German-Israeli Research Program and the Wolfson and Minerva Foundations.

Received July 28, 1999; revised October 15, 1999.

References

Arieli, A., Shoham, D., Hildesheim, R., and Grinvald, A. (1995). Coherent spatiotemporal patterns of ongoing activity revealed by real-time optical imaging coupled with single-unit recording in the cat visual cortex. J. Neurophysiol. *73*, 2072–2093.

Arieli, A., Sterkin, A., Grinvald, A., and Aertsen, A. (1996). Dynamics of ongoing activity: explanation of the large variability in evoked cortical responses. Science *273*, 1868–1871.

Blasdel, G.G., and Salama, G. (1986). Voltage-sensitive dyes reveal a modular organization in monkey striate cortex. Nature *321*, 579–585.

Bonhoeffer, T., and Grinvald, A. (1993). The layout of iso-orientation domains in area 18 of cat visual cortex: optical imaging reveals a pinwheel-like organization. J. Neurosci. *13*, 4157–4180.

Bonhoeffer, T., and Grinvald, A. (1996). Optical imaging based on intrinsic signals—the methodology. In Brain Mapping: The Methods, A.W. Toga and J.C. Mazziotta, eds. (New York: Academic Press), pp. 55–97.

Cacciatore, T.W., Brodfuehrer, P.D., Gonzalez, J.E., Jiang, T., Adams, S.R., Tsien, R.Y., Kristan, W.B., and Kleinfeld, D. (1999). Identification of neural circuits by imaging coherent electrical activity with FRET-based dyes. Neuron *23*, 449–459.

Cohen, L.B. (1973). Changes in neuron structure during action potential propagation and synaptic transmission. Physiol. Rev. *53*, 373–418.

Cohen, L.B., Keynes, R.D., and Hille, B. (1968). Light scattering and birefringence changes during nerve activity. Nature *218*, 438–441.

Cohen, L.B., Salzberg, B.M., Davila, H.V., Ross, W.N., Landowne, D., Waggoner, A.S., and Wang, C.H. (1974). Changes in axon fluorescence during activity: molecular probes of membrane potential. J. Membr. Biol. *19*, 1–36.

Fluhler, E., Burnham, V.G., and Loew, L.M. (1985). Spectra, membrane binding, and potentiometric responses of new charge shift probes. Biochemistry *24*, 5749–5755.

Frostig, R.D., Lieke, E.E., Ts'o, D.Y., and Grinvald, A. (1990). Cortical functional architecture and local coupling between neuronal activity and the microcirculation revealed by in vivo high-resolution optical imaging of intrinsic signals. Proc. Natl. Acad. Sci. USA *87*, 6082–6086.

George, J.S., Aine, C.J., Mosher, J.C., Schmidt, D.M., Ranken, D.M., Schlitt, H.A., Wood, C.C., Lewine, J.D., Sanders, J.A., and Belliveau, J.W. (1995). Mapping function in the human brain with magnetoencephalography, anatomical magnetic resonance imaging, and functional magnetic resonance imaging. J. Clin. Neurophysiol. *12*, 406–431.

Gonzalez, J.E., and Tsien, R.Y. (1997). Improved indicators of cell membrane potential that use fluorescence resonance energy transfer. Chem. Biol. *4*, 269–277.

Grinvald, A., and Farber, I.C. (1981). Optical recording of calcium action potentials from growth cones of cultured neurons with a laser microbeam. Science *212*, 1164–1167.

Grinvald, A., Salzberg, B.M., and Cohen, L.B. (1977). Simultaneous recording from several neurones in an invertebrate central nervous system. Nature *268*, 140–142.

Grinvald, A., Cohen, L.B., Lesher, S., and Boyle, M.B. (1981). Simultaneous optical monitoring of activity of many neurons in invertebrate ganglia using a 124-element photodiode array. J. Neurophysiol. *45*, 829–840.

Grinvald, A., Hildesheim, R., Farber, I.C., and Anglister, L. (1982a). Improved fluorescent probes for the measurement of rapid changes in membrane potential. Biophys. J. *39*, 301–308.

Grinvald, A., Manker, A., and Segal, M. (1982b). Visualization of the spread of electrical activity in rat hippocampal slices by voltage-sensitive optical probes. J. Physiol. (Lond.) *333*, 269–291.

Grinvald, A., Fine, A., Farber, I.C., and Hildesheim, R. (1983). Fluorescence monitoring of electrical responses from small neurons and their processes. Biophys. J. *42*, 195–198.

Grinvald, A., Anglister, L., Freeman, J.A., Hildesheim, R., and Manker, A. (1984). Real-time optical imaging of naturally evoked electrical activity in intact frog brain. Nature *308*, 848–850.

Grinvald, A., Lieke, E., Frostig, R.D., Gilbert, C.D., and Wiesel, T.N. (1986). Functional architecture of cortex revealed by optical imaging of intrinsic signals. Nature *324*, 361–364.

Grinvald, A., Frostig, R.D., Lieke, E.E., and Hildesheim, R. (1988). Optical imaging of neuronal activity. Physiol. Rev. *68*, 1285–1366.

Grinvald, A., Lieke, E.E., Frostig, R.D., and Hildesheim, R. (1994). Cortical point-spread function and long-range lateral interactions revealed by real-time optical imaging of macaque monkey primary visual cortex. J. Neurosci. *14*, 2545–2568.

Grinvald, A., Shoham, D., Shmuel, A., Glaser, D.E., Vanzetta, I., Shtoyerman, E., Slovin, H., Wijnbergen, C., Hildesheim, R., Sterkin, A., and Arieli, A. (1999). In-vivo optical imaging of cortical architecture and dynamics. In Modern Techniques in Neuroscience Research, U. Windhorst and H. Johansson, eds. (Heidelberg: Springer-Verlag), pp. 894–969.

Gupta, R.K., Salzberg, B.M., Grinvald, A., Cohen, L.B., Kamino, K., Lesher, S., Boyle, M.B., Waggoner, A.S., and Wang, C.H. (1981). Improvements in optical methods for measuring rapid changes in membrane potential. J. Membr. Biol. *58*, 123–137.

Hill, D., and Keynes, R.D. (1949). Opacity changes in stimulated nerve. J. Physiol. *108*, 278–281.

Iijima, T., Witter, M.P., Ichikawa, M., Tominaga, T., Kajiwara, R., and Matsumoto, G. (1996). Entorhinal–hippocampal interactions revealed by real-time imaging. Science *272*, 1176–1179.

Kauer, J.S. (1988). Real-time imaging of evoked activity in local circuits of the salamander olfactory bulb. Nature *331*, 166–168.

Kauer, J.S., Senseman, D.M., and Cohen, L.B. (1987). Odor-elicited activity monitored simultaneously from 124 regions of the salamander olfactory bulb using a voltage-sensitive dye. Brain Res. *418*, 255–261.

Loew, L.M., Bonneville, G.W., and Surow, J. (1978). Charge shift optical probes of membrane potential. Theory Biochem. *17*, 4065–4071.

Miyawaki, A., Llopis, J., Heim, R., McCaffery, J.M., Adams, J.A., Ikura, M., and Tsien, R.Y. (1997). Fluorescent indicators for Ca^{2+} based on green fluorescent proteins and calmodulin. Nature *388*, 882–887.

Nicolelis, M.A., Ghazanfar, A.A., Faggin, B.M., Votaw, S., and Oliveira, L.M. (1997). Reconstructing the engram: simultaneous, multisite, many single neuron recordings. Neuron *18*, 529–537.

Orbach, H.S., Cohen, L.B., and Grinvald, A. (1985). Optical mapping of electrical activity in rat somatosensory and visual cortex. J. Neurosci. *5*, 1886–1895.

Ratzlaff, E.H., and Grinvald, A. (1991). A tandem-lens epifluorescence macroscope: hundred-fold brightness advantage for wide-field imaging. J. Neurosci. Methods *36*, 127–137.

Ross, W.N., Salzberg, B.M., Cohen, L.B., Grinvald, A., Davila, H.V., Waggoner, A.S., and Wang, C.H. (1977). Changes in absorption, fluorescence, dichroism, and birefringence in stained giant axons: optical measurement of membrane potential. J. Membr. Biol. *33*, 141–183.

Salzberg, B.M., Davila, H.V., and Cohen, L.B. (1973). Optical recording of impulses in individual neurones of an invertebrate central nervous system. Nature *246*, 508–509.

Salzberg, B.M., Grinvald, A., Cohen, L.B., Davila, H.V., and Ross, W.N. (1977). Optical recording of neuronal activity in an invertebrate central nervous system: simultaneous monitoring of several neurons. J. Neurophysiol. *40*, 1281–1291.

Shoham, D. (1997). Images of sensation: studies of functional architecture and dynamic activity patterns in sensory cortex, using optical imaging techniques. PhD thesis, Weizmann Institute of Science, Rehovat, Israel.

Siegel, M.S., and Isacoff, E.Y. (1997). A genetically encoded optical probe of membrane voltage. Neuron *19*, 735–741.

Tasaki, I., Watanabe, A., Sandlin, R., and Carnay, L. (1968). Changes in fluorescence, turbidity and birefringence associated with nerve excitation. Proc. Natl. Acad. Sci. USA *61*, 883–888.

Ts'o, D.Y., Frostig, R.D., Lieke, E.E., and Grinvald, A. (1990). Functional organization of primate visual cortex revealed by high resolution optical imaging. Science *249*, 417–420.